

Modeling, testing and validation of the vibrational behavior of a dynamometric test rig for railway braking systems

Luca Pugi and Giulio Rosano

Department of Industrial Engineering, University of Florence, Florence, Italy, and

Riccardo Viviani, Leonardo Cabrucci and Luca Bociolini

Italcertifer SPA, Florence, Italy

Abstract

Purpose – The purpose of this work is to optimize the monitoring of vibrations on dynamometric test rigs for railway brakes. This is a quite demanding application considering the continuous increase of performances of high-speed trains that involve higher testing specifications for brake pads and disks.

Design/methodology/approach – In this work, authors propose a mixed approach in which relatively simple finite element models are used to support the optimization of a diagnostic system that is used to monitor vibration levels and rotor-dynamical behavior of the machine. The model is calibrated with experimental data recorded on the same rig that must be identified and monitored. The whole process is optimized to not interfere with normal operations of the rig, using common inertial sensor and tools and are available as standard instrumentation for this kind of applications. So at the end all the calibration activities can be performed normally without interrupting the activities of the rig introducing additional costs due to system unavailability.

Findings – Proposed approach was able to identify in a very simple and fast way the vibrational behavior of the investigated rig, also giving precious information concerning the anisotropic behavior of supports and their damping. All these data are quite difficult to be found in technical literature because they are quite sensitive to assembly tolerances and to many other factors. Dynamometric test rigs are an important application widely diffused for both road and rail vehicles. Also proposed procedure can be easily extended and generalized to a wide value of machine with horizontal rotors.

Originality/value – Most of the studies in literature are referred to electrical motors or turbomachines operating with relatively slow transients and constant inertial properties. For investigated machines both these conditions are not verified, making the proposed application quite unusual and original with respect to current application. At the same time, there is a wide variety of special machines that are usually marginally covered by standard testing methodologies to which the proposed approach can be successfully extended.

Keywords Identification, Bearing, Modal analysis, Mechatronics, Dynamometric test rig, Vibration monitoring, Identification of roller bearings

Paper type Case study

Nomenclature

a_i = acceleration of the i -th point;
 f_1, f_2, f_r = half power frequencies and resonance for half power method;
 F_c = total clamping force applied on brake pad;
 $k_{xx\ i}$ = stiffness of the i -th bearing along direction x ;
 $k_{yy\ i}$ = stiffness of the i -th bearing along direction y ;
 $k_{xy\ i}$ = extra diagonal cross-stiffness of the i -th bearing;
 I_m = mechanical inertia of the rig;
 I_{ref} = inertia that must be emulated by the rig;
 M_b = braking torque applied on tested brake pad and disc;
 M_e = torque provided by electric motor of the test rig;
 r_b = braking radius of tested brake disc;
 v_i = speed/velocity of the i -th measurement point;

$v_{i\ j}$ = j -th component of speed/velocity of the i -th measurement point;
 $v_{i\ rms}$ = rms of the speed of the i -th measurement point;
 $v_{i\ j\ rms}$ = rms of the j -th component of speed of the i -th measurement point;
 x_g, y_g = transversal, vertical position of the center of mass;
 x_b, y_b = transversal and vertical displacements of the i -th supports of the test rig;
 x_m, ψ_m = mean and scaled difference of transversal displacements of supports 3 and 4;

The current issue and full text archive of this journal is available on Emerald Insight at: <https://www.emerald.com/insight/1708-5284.htm>



World Journal of Engineering
21/3 (2024) 425–442
Emerald Publishing Limited [ISSN 1708-5284]
[DOI 10.1108/WJE-07-2022-0298]

© Luca Pugi, Giulio Rosano, Riccardo Viviani, Leonardo Cabrucci and Luca Bociolini. Published by Emerald Publishing Limited. This article is published under the Creative Commons Attribution (CC BY 4.0) licence. Anyone may reproduce, distribute, translate and create derivative works of this article (for both commercial and non-commercial purposes), subject to full attribution to the original publication and authors. The full terms of this licence may be seen at <http://creativecommons.org/licenses/by/4.0/> legalcode

Received 23 July 2022
Revised 26 November 2022
Accepted 3 January 2023

- ξ = damping factor of a mode;
- θ, φ = orientation angles;
- Y_{ij} = rms of the j-th component of speed measurement on the i-th measurement point with respect to the squared value of the rig speed Ω ;
- μ = friction factor between brake pad and disc;
- ω = frequency of measured displacement, speed or accelerations; and
- Ω = rotational speed of the rig.

1. Introduction

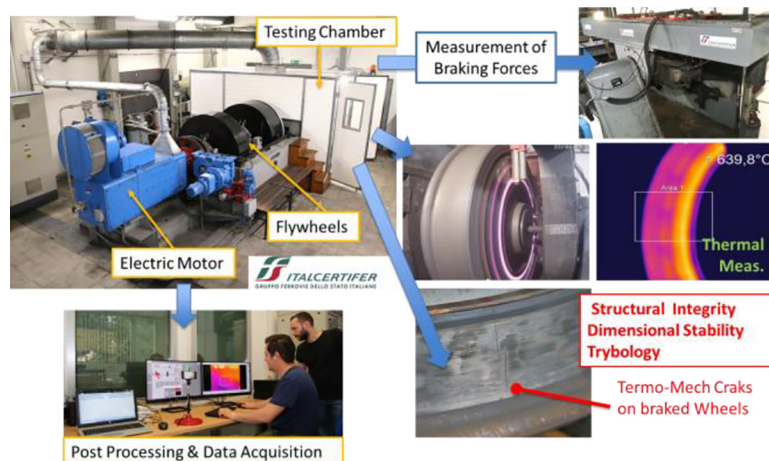
Braking performances play a key role for the safety of railway systems (Pugi et al., 2015).

Eligibility (UIC 541-3: Brakes, 2017) and Reliability (IRS50548, 2020) of friction materials used for brakes must be verified on dedicated test rigs (Presciani et al., 2003; Borawski, 2019), the so-called dynamometric test rigs. These rigs, as shown in examples of Figures 1 and 2, are composed by rotors with a variable set of flywheels that are needed to emulate the equivalent inertia of the vehicle. Vibrational behavior of these machines must be carefully monitored without affecting their usage which involves the uninterrupted execution of thousands of braking tests every year.

Despite the complexity of the problem, aim of this work is the development of a simple procedure that should be used for a fast identification of the vibrational behavior of a widely diffused class of machines. Applicable standards as ISO 20816-1 (2016) are mainly referred to the evaluation of vibration on supports of continuously rotating machines with constant inertia such as electrical motors, generators and turbomachines. So, there is a substantial lack of preexisting literature regarding methodologies that can be applied to machines like dynamometric test rigs which are subjected every year to thousands of accelerating and decelerating transients with variable inertial properties and testing conditions.

Safety and productivity of these machines are important for both railway and automotive industries because these test rigs are indispensable for different research topics and industrial applications:

Figure 1 Dynamometric test rig for brake friction materials



Source: Images from Italcertifer Rig via Lanzi in Florence, Italy

Figure 2 New dynamometric test rig for high speed at RFI CDSO in Osmannoro (Florence, Italy)



- New braking materials (Bian and Wu, 2016);
- Brake related, particle pollution (Alemani et al., 2018);
- Identification friction (EHret, 2021; Sawczuk et al., 2021), wear (Yanar et al., 2022; Kim et al., 2021) and squealing models (Bracciali and Megna, 2018); and
- Optimized thermo-structural and fluid dynamics behavior (Sawczuk and Jüngst, 2019; Yevtushenko et al., 2019).

So the development of tailored procedures for the evaluation of their vibrational behavior on supports is justified.

The innovative contribution of this work is represented by the possibility of defining a testing and identification procedures that should be performed with null or negligible impact on the normal activities of the rig. Identification of expected modal behavior is also very useful for the definition of the measurement layout (accelerometer/velocimeters) that should be used to monitor the rig, also giving precious indications for the interpretation of acquired data.

So, this is a small but significant contribution to improve quality and safety of testing activities for important kind of rigs. This study is applied to a real important test case, the dynamometric test rig of Italcertifer Spa shown in Figure 1. Investigated test case is one of the few rigs homologated by UIC (International Union of Railways), as described in Table 1.

So, it can be concluded that also the proposed test case is quite significative with respect to the current state of the art.

The number of rigs used for railway brakes including not homologated ones should be evaluated in about one hundred or more. Automotive and motorbike market are far larger than

Table 1 List of UIC homologated test rig in the world (UIC 548 Brakes, 2020)

Class*	Rig owner/ location	Date of last approval	Expiry date
D/K/I	DB/ Minden (Germany)	Jan 1998	Jan 2025
D/K/I	Italcertifer/Florence (Italy)	Jan 1999	Jan 2025
D/K/I	PKP/ Warsaw (Poland)	Jan 2001	Jan 2025
D/K/I	SNCF(MF1)/ Vitry (France)	Jan 1998	Jan 2025
D/K/I	SNCF(MF3)/ Vitry (France)	Jan 1998	Jan 2025
D/K/I	ZZSK/Zilina (Slovakia)	Jan 2001	Jan 2025
K/I	RTA/Wien (Austria)	Jan 2015	Jan 2020
D/I	CARS/Beijing (China)	Jun 2018	Jun 2023
K/M	Fed.Mogull/Glinde (Germany)	Jun 2011	Jan 2025
D/M	Fed.Mogull/Glinde (Germany)	Jan 2012	Jan 2025
K/M	Wabtec/Avellino (Italy)	Jan 2019	Jul 2024
D/M	Wabtec/Avellino (Italy)	Jan 2013	Jul 2025
D/M	Flertex/Genevilliers (France)	Apr 2013	Apr 2024
K/M	ICER/Pamplona (Spain)	Apr 2015	Apr 2025
D/M	Knorr-Bremse/ Munich (Germany)	Jan 2013	Jan 2025
D/K/M	Akebono/ Hanyu (Japan)	Jul 2020	Jul 2025

the railway one. So, the number of installed rigs is not recorded so precisely but it is far higher: even in a single automotive R&D site like Brembo or Kilometro Rosso ones (Bergamo, Italy) tenths of full-scale rigs are installed. Results of this study can be extended to other classes of horizontal rotors supported by roller bearings with variable preloads.

2. Dynamometric test rigs for railway brakes: description, state of the art and proposed identification procedure

2.1 Layout and functionalities of a dynamometric test rig

As shown in Figures 1 and 2, a dynamometric test rig is composed by a rotor moved by an electric motor that is equipped with an array of different flywheels.

Flywheels are used to modify the simulated inertia and consequently the energy that is dissipated by the tested brake pad (Shuai et al., 2019; Lyu et al., 2018).

If the inertia I_{ref} that must be simulated by the test rig is different from the rig inertia I_m , the electric motor must provide a compensating torque M_e . M_e is proportional to applied braking torque and to the relative error between real and desired inertia (1):

$$M_e = M_b \left(\frac{I_m - I_{ref}}{I_{ref}} \right) \quad (1)$$

Following mechanical measurements are often performed:

- Measurement of applied clamping forces (F_c) and braking torque (M_b): from these measurements it is evaluated the friction factor μ between tested pad and disc (2); r_b is the equivalent mean braking radius of the disc.

$$M_b = \mu r_b F_c \Rightarrow \mu = \frac{M_b}{r_b F_c} \quad (2)$$

- Temperatures: thermal behavior of tested elements is typically verified with direct measurements (thermocouples).

Additional measurements are performed with infrared sensors and cameras.

- Wear of pads: simulated braking tests are performed to dissipate a known energy; wear of pads is measured in terms of weight loss. In this way, it is possible to calculate a wear ratio coefficient k_w , typically expressed in cm^3 of worn material with respect to dissipated energy expressed in MJ. Value of k_w is about 0.3–0.6 cm^3/MJ . Growing interest is also related to the dimensional and chemical analysis of worn debris to evaluate their impact on health and surrounding environment (Gehrig et al., 2007). This topic is quite important for closed spaces such as metro-stations in tunnels (Mann et al., 2021). A comparison between new brake pads and worn ones (after testing) is shown in Figure 3.
- Structural integrity dimensional stability: braked discs and wheels are subjected to heavy thermo-mechanical loads (Wang et al. 2019). So structural integrity and dimensional stability of these components must be verified. Wear, roughness and tribological features such as generation of micro-cracking are also investigated (Fan, 2021; Wang et al. 2015).

Figure 3 Examples of sintered brake pads tested at Italcertifer test rig

2.2 Certification and homologation of railway dynamometric test rigs

Dynamometric test rigs are used to verify and homologate brake friction materials and components. Considering legal and economic consequences of performed testing activities, also performances of test rigs must be certified according to international standards such as [IRS50548 \(2020\)](#). The most important verification that a test rig must pass is the so-called “round robin test”: performances of the rig that must be approved are compared with a set of experimental results that have been previously evaluated on a homologated test rig: to perform this comparison, identical specimens are tested on both rigs performing the same test program. The same tests performed on different rigs must produce within acceptable tolerances, the same results. These tests are repeated periodically to monitor the state of the system with aging or respect to significant updates of the device. All these activities are subjected to various level of control and verification, including inspections of designed international committees. Testing programs are periodically updated to take count of technological improvement of braking technology. So, requirements for this kind of devices are generally subjected to periodic revisions. As a part of this trend, requirements regarding the amount of dissipated energy and max operational speed are generally increasing. As example, testing programs of sintered brake pads for high-speed trains (visible in [Figure 2](#)) currently involve the simulation of brake maneuvers from a maximum speed of 500 km/h. Operational life of rigs is typically very long (tenths of years), with periodical updates of both expected functionalities and specifications that must be verified to maintain the homologation of the rig. It is quite common for a rig’s consistent increase of operational speed and managed braking energies during its life. So, it’s not unusual for a mature test rig to work frequently in near to off-design conditions with respect to their original specifications. Motors, sensors and many other components are often updated, but interventions on the mechanical layout of these rigs are difficult to be performed. All these considerations lead to the conclusion that vibration monitoring plays a key role in assuring safety, and an acceptable increase of the operational life of this kind of machines.

2.3 Monitoring of vibrations transmitted to supports: state of the art and adopted solutions

For vibration monitoring of dynamometric test rig for railway brakes, a specific literature is near to be completely absent.

Recent works ([Duan et al.2018](#); [Malla and Panigrahi, 2019](#)) suggest some general techniques for the analysis of vibrations of roller bearings and their possible correlation with various kind of defects of rolling elements, cages, outer and inner races. Most of these review papers focus their attention on various kinds of signal analysis related to spectral content of three kinds of sensors:

- accelerometers ([Donelson and Dicus, 2002](#)), velocimeters, etc: direct measurements of accelerations or other derived indexes are performed directly with sensors on supports;
- eddy current and more general relative displacement measurements ([Dadouche et al, 2008](#)); and

- acoustic measurements: acoustic emissions are correlated to specific phenomena within the bearing ([Hemmati et al., 2016](#));

The first method based on inertial measurement of support vibration is more diffused for heavy machineries such as rolling mills ([Nirwan and Ramani, 2022](#)) or electrical machines. These applications are like the proposed one in terms of size, speed and adopted components. Monitoring of dynamometric test rig, as the Italcertifer one, is currently performed using velocimeters on supports. Adopted sensors are described in [Figure 4](#): a single velocimeter is used for each support mainly measuring vibration in vertical direction.

Equivalent RMS values v_{rms} (3) are calculated according to general standards ([ISO 20816-1, 2016](#)): these standards define v_{rms} thresholds to activate maintenance or emergency procedures:

$$v_{rms} = \frac{1}{\sqrt{2}} \sqrt{\int_{10 \times 2\pi}^{1000 \times 2\pi} v^2(\omega) d\omega} = \frac{1}{\sqrt{2}} \sqrt{\int_{10 \times 2\pi}^{1000 \times 2\pi} \left(\frac{a(\omega)}{\omega}\right)^2 d\omega} \quad (3)$$

$v(\omega)$ and $a(\omega)$ are the spectra of speed and acceleration with respect to the frequency ω measured on each monitored support. RMS is evaluated within a frequency range from 10 to 1,000 Hz.

This is a general approach that is adopted by tools provided by the same suppliers of bearings ([Fag Pro Check Monitoring System, 2022](#); [Simpro Quick Pro, 2022](#)).

However, dynamometric test rigs present several features that are quite uncommon with respect to more diffused and probably more studied applications.

The machine is used to simulate multiple braking maneuvers, therefore, resulting speed profile is a sequence of acceleration and deceleration transients. For the same reason the machine is subjected to torsional transients.

Finally, the machine is substantially a horizontal shaft composed of modular sections which sustain heavy flywheels. Radial preloads cause an anisotropic behavior of bearings which are also supported by a basement which is not strictly isotropic with respect to excitations in vertical or transversal directions. Preloads are variable according to simulated inertia so the whole system is affected by strong parametric variations.

Studies for rigid ([Tomovic et al., 2010](#)) and flexible rotors ([Kurvinen et al., 2020](#)) with compliant bearings have been recently published: comprehension of excited modal shapes including anisotropic effects is also fundamental for a proper placement of sensors on supports and a correct estimation of the vibration levels ([Randall, 2021](#)). This technical literature was the starting point for the identification of the procedure proposed in this work.

2.4 Proposed identification procedure

As shown in [Figure 5](#), proposed identification procedure is organized in the following phases:

- 1 Simplified finite element model: a finite element model of the rig is assembled as described in Section 3 of this work. Preliminary results of this modeling phase are used to

Figure 4 Example of installed velocimeters on supports (Italcertifer test rig via Lanzi)


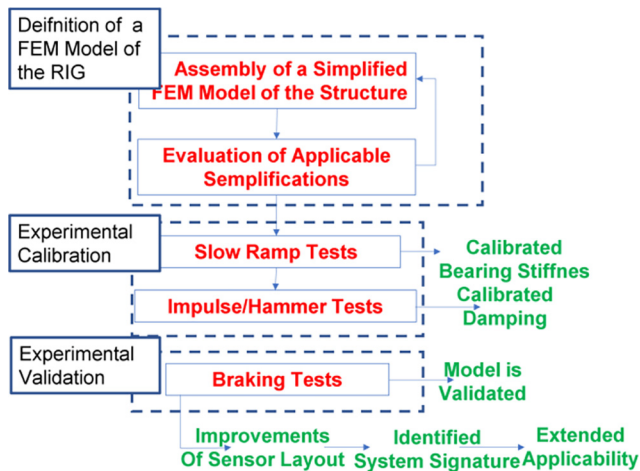
Property	Value	Image
Sensitivity	21.2 mV/mms ⁻¹	
Range(disp.)	± 1 mm	
Freq. Range	10÷1000 Hz	
Res. Frequency	12Hz	
Damping (1st mode)	07	
Transv. Sensitivity	<7%	
Model	CEMB T1-40	

Figure 5 Flowchart of proposed identification procedure

evaluate what simplifications can be reasonably introduced to optimize the execution of the FEM model:

- Rotor flexibility: if flexible behavior of the rotor is weakly excited, faster, but less precise modeling of the rotor with beam elements can be adopted.
 - Gyroscopic effects: if gyroscopic effects are negligible, positioning of eigen-frequencies and modes is not influenced by the speed of the rotor.
 - Nonlinear behavior of bearings: nonlinear/anisotropic behavior of bearings affects the response of the machine especially for what concern low frequency modes.
- 2 Experimental model calibration: FEM model is calibrated by identifying model parameters that are affected by higher uncertainties, such as equivalent bearing stiffness and damping:
- Slow ramp tests: by identifying the modal response of the rig during slow acceleration phases, it is possible to roughly calibrate the estimated stiffness of bearings in different directions.
 - Impulse tests: damping of the system is identified with static impulse tests performed with impulsive excitations exploiting the so-called half power method (Ewins, 2009).
 - Experimental model validation with braking tests: during braking tests both flexural and torsional behavior of the rig is excited with fast transients. In this way, performed identification is evaluated over a population of test that is completely different from the one used for calibration.

Conclusions and suggested improvements of monitoring system and general extension of proposed methodologies:

over-described activities are used to further improve the way in which the system is monitored. Results of the activities performed on the benchmark test rig of Italcertifer give some indications for the extension of proposed methodologies to other test rigs, such as the new high-speed one described in Figure 2 that is designed to simulate braking speed exceeding 500 km/h.

3. Finite element modeling

In Figure 6(a), main elements of Italcertifer rig are shown: the rig is composed by two flanged shafts sustained by roller bearings (FAG model 22238-MB) connected with motor through elastic joints. Three different flywheels can be flanged to the shaft to reproduce eight different values of mechanical inertia that can be further regulated by the electrical torque of the motor. Flywheels named “2” and “3” in Figure 6 are flanged to the first shaft briefly called “motor shaft.” The other flywheel the “4” is flanged on the second shaft also called “spindle shaft.”

This kind of structure is common to almost the whole population of existing and homologated dynamometric test rigs (as listed in Table 1). Aim of this work is to produce a simple finite element model that should be applied with minimal modifications (number and dimensions of flywheels, bearing model, etc.) to other existing devices.

The finite model of the rig is visible in Figure 6(b): the shaft is modeled as a Bernoulli beam in which the inertial contributions of different sections and flywheels are introduced. Adoption of a Bernoulli beam model should introduce some approximations for what concern the flexible behavior of the rig and it is preferred to more sophisticated approaches only for two reasons: maximum simplification of proposed model and acceptable approximations especially for low frequency modes which are mostly rigid ones.

Bearings are modeled as lumped viscous-elastic elements connecting the rotor with the basement. The rotor is subjected to vertical preloads due to the weight of flywheels and is relatively unloaded with respect to transversal and axial forces. For these reasons, variations of stiffness associated to different preload applied on joints cannot be ignored: data on variable stiffness of bearings are taken from engineering tools available online.

Most complete data have been supplied by SKF; SKF is not the supplier of the bearings currently installed (which is FAG), but it produces an almost equivalent product.

It was not possible to measure assembly tolerances and preloads on the machine without disassembling it; data in Figure 7 are referred to estimated stiffness of the bearing with no additional preloads. This was considered the most cautious hypothesis but clearly not the most realistic one. For what

Figure 6 (a) Italcertifer test rig and (b) corresponding finite element model

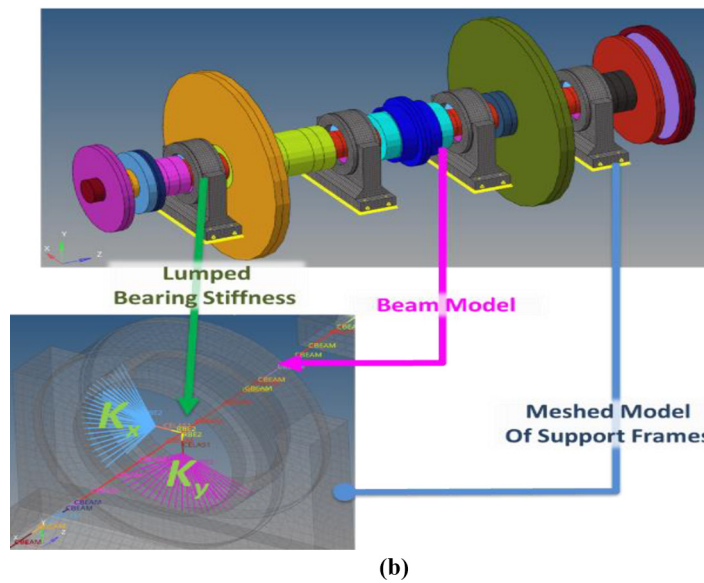
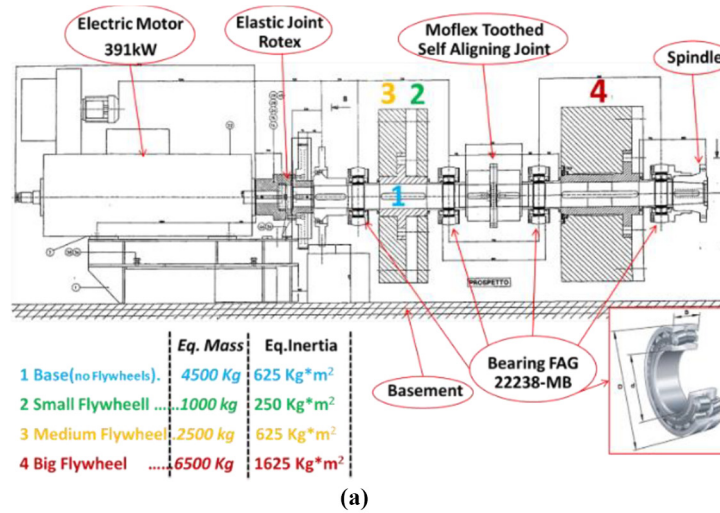
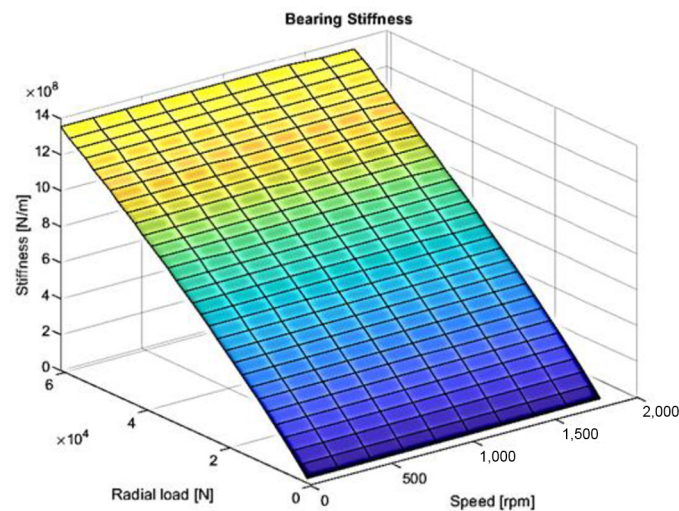


Figure 7 Simulated stiffness behavior according to data from SIMPRO Quick™ software (no preload on bearings)



concerns the stiffness matrix K is supposed a diagonal one (cross-interactions are neglected) in which both vertical k_{yy} and horizontal k_{xx} stiffness of the bearing are modeled with an equal radial (equal) radial stiffness k_r . k_r is tabulated with respect to applied loads (weight and unbalance in x and y directions) and speed, as visible in [Figure 7](#).

Supports and basement are modeled with a large mesh to roughly implement some equivalent compliance of the structure under the bearings. For what concerns elastic joints, authors found indications concerning their axial and transversal stiffness that almost confirm their limited capacity of transmitting appreciable “not torsional” loads along the structure.

Proposed model was used to perform a preliminary rotor-dynamic analysis to understand the modal behavior of the system. Analysis is performed considering the applications to both shafts of the minimum inertia, as this configuration is the only currently used to reach the highest working speed of the rig. Modal behavior is studied until a maximum frequency of 300 Hz. This value corresponds to the 12th harmonics of synchronous excitation for the maximum speed of the rig (1,500 rpm equal to 25 Hz).

A Campbell diagram of rotor behavior obtained with the FEM model is shown in [Figure 8](#):

- There are some torsional modes which are substantially decoupled with respect to the other ones. Especially the first torsional is mainly associated to compliance of flexible joints between various parts of the rig.
- There is a strong decoupling between modes affecting both shafts of the rig as flexible joints between shafts have an almost negligible bending stiffness with respect to connected elements.
- Flexible behavior of the shaft is associated only to high frequency phenomena over 180 Hz. Gyroscopic effects weakly affect flexible modes over 180–200 Hz; most of the dynamic behavior of the rig can be explained using simpler approaches ([Ewins, 2009](#)), as the modal superposition principle ([Pugi and Abati, 2020](#)), introducing relatively small errors. Also, it is quite evident that errors introduced by the adoption of Bernoulli beam model are quite negligible.
- Modes under 180 Hz are substantially rigid motions of the shafts due to compliances of bearings. Transversal and vertical bouncing and tilting modes are almost decoupled. This behavior is justified by the effect of the vertical preload assured by the weight of shafts and flanges: bearings are stiffer in vertical direction “Y” with respect to the horizontal one, “X.”
- For both shafts, both vertical and transversal modes should be interpreted in terms of planar bouncing and tilting motions as visible in [Figure 9](#): a first mode at 21 Hz can be roughly approximated to an alternate yaw rotation of the shaft around its center of mass so it is defined as tilting mode. The second mode at 25 Hz can be approximated as a planar alternate translation of the shaft, so it is called bouncing mode. Vertical modes have similar shapes but much higher frequencies (80 and 95 Hz) as vertical stiffness of supports is much higher than horizontal one.

These preliminary results are useful to understand the modal behavior of the rig, but they are numerically inaccurate, as

simulation results demonstrate that dynamic behavior of the rig is influenced by bearings: data used for bearings are referred to another manufacturer. Also, effective stiffness of the bearings is strongly influenced by assembly tolerances and by mounting preloads. These parameters are quite impossible to be verified on a preexisting machine without disassembling it. Data of [Figure 6](#) are referred to a bearing which is not preloaded so preliminary values inserted in the model are cautious but probably underestimated. So, an experimental campaign has been arranged to refine these preliminary calculations especially for what concern equivalent stiffness and damping of supports.

4. Experimental campaign: model calibration

Finite element model has given indications on the dynamic behavior of the rig both in terms of expected modes and of applicable methodologies: the dynamical behavior of the rig is strongly affected by bearings and by assembly tolerances which were substantially unknown.

So, it was arranged as experimental campaign to perform an identification. The rig was equipped with MEMS accelerometers placed on supports as described in [Figure 10](#) and in [Table 2](#): accelerations on both vertical and transversal directions are recorded. Additional measurements on motors and foundations have been performed. According to standards, measurements are sampled and filtered to assure a bandwidth of 1,000 Hz.

Testing campaign was organized in the following ways:

- Slow ramp tests: the rig is slowly accelerated and decelerated without applying any braking load: aim of these tests is to evaluate the steady-state response of the rig with respect to its natural unbalance with variable speed.
- Impulse response tests: impulse excitation is applied to the machine in standstill conditions.
- Braking tests: vibrations and more generally the modal behavior of the machine is verified during a braking test.

4.1 Slow ramp tests

The rig is slowly accelerated to evaluate a continuous identification of the rig frequency response with respect to speed. Vibrations are measured with accelerometers described in [Table 2](#). Measured accelerations are self-excited by rotor unbalance; so tests are performed considering a repeatable excitation which is only approximately known. Most of these tests are performed with the minimum inertia visible in [Figure 11](#) that is adopted to reach the maximum speed. Tests are repeated considering a constant slow deceleration from maximum speed to zero. Ramp transients introduce a distortion of the measured spectrum which is increasing with respect to applied acceleration and deceleration. These distortions produce a frequency shift ([Ewins, 2009](#)) on measured spectrum of accelerations of investigated machine. Frequency shift can be evaluated by comparing spectral analyses performed with increasing or decreasing speed of the rig. Frequency shift is more evident for low frequencies of the spectrum; calibration was optimized for a range of frequencies between 10 and 200 Hz considering a rig speed between 1,000 and 1,500 rpm.

This optimization also depends on chosen acquisition parameters that are described in [Table 3](#). For this reason, tests

Figure 8 Campbell diagram and classification of calculated modes of Italcertifier test rig

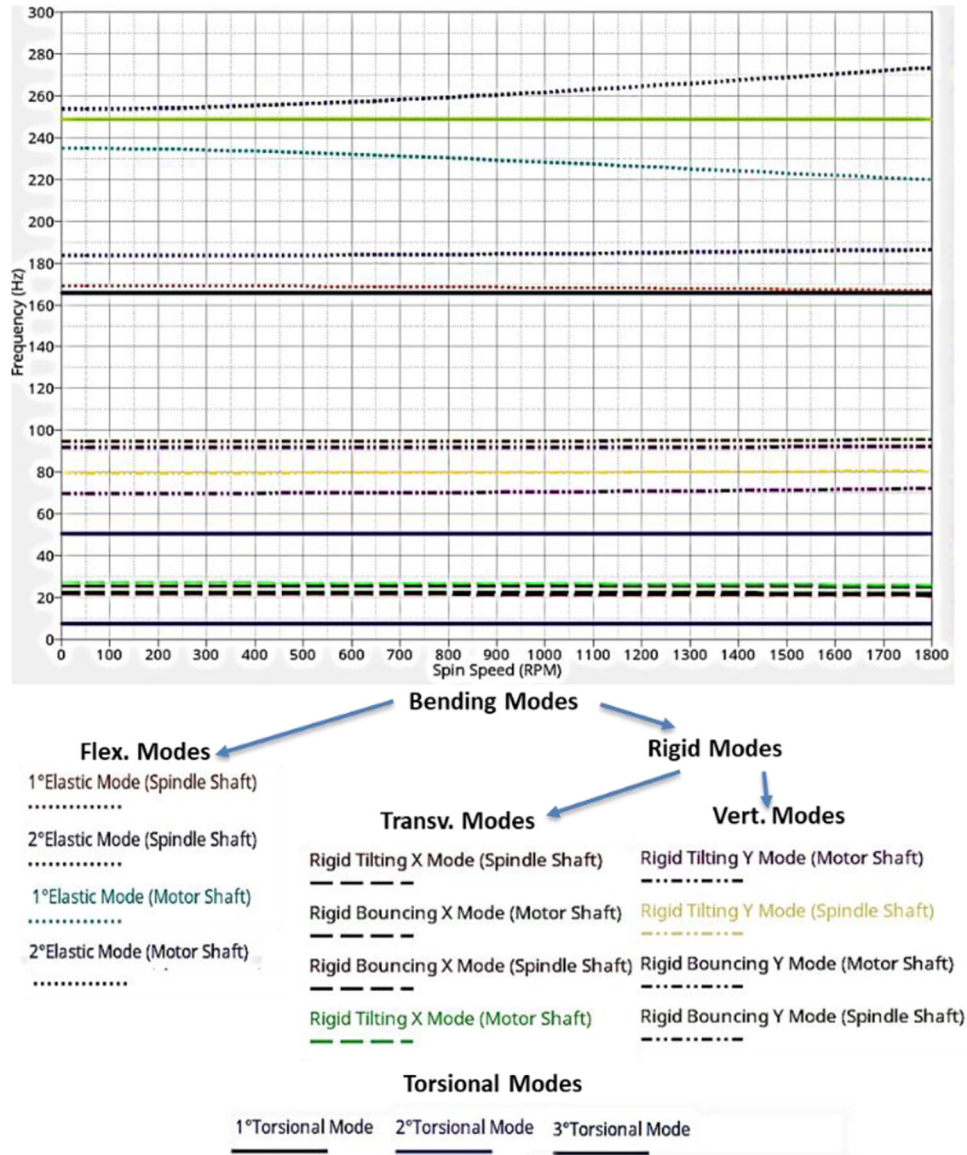


Figure 9 Comparison of tilting and bouncing mode of a shaft along the transversal plane ("x" direction)

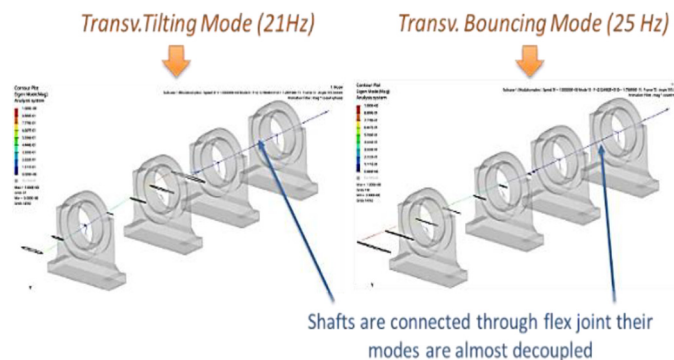


Figure 10 Layout of installed accelerometers

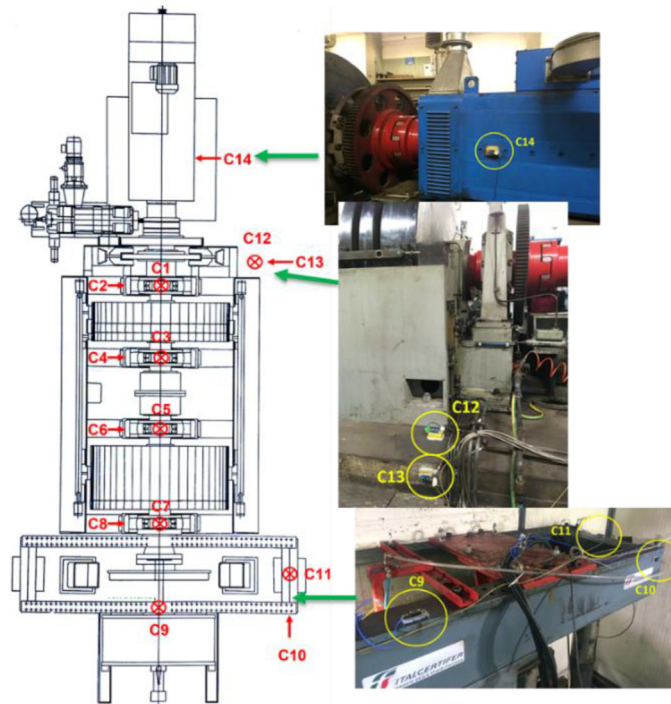


Table 2 Layout of accelerometers for the testing campaign

N	Position	Model	Range (g)	Sensitivity [mV/(m/s ²)]
C1	Vertical bearing 1	PCB 3741B1210G	10	20.40
C2	Horizontal bearing 1	PCB 3741B1210G	10	20.40
C3	Vertical bearing 2	PCB 3741B1210G	10	20.40
C4	Horizontal bearing 2	PCB 3741B1210G	10	20.40
C5	Vertical bearing 3	PCB 3741B1210G	10	20.40
C6	Horizontal bearing 3	PCB 3741B1210G	10	20.40
C7	Vertical bearing 4	ASC 4421MF-010G	10	27.50
C8	Horizontal bearing 4	ASC 4421MF-010G	10	27.50
C9	Central Prony vertical	ASC 4421MF-010G	10	27.50
C10	Lateral Prony horizontal	PCB 3741B1210G	10	20.40
C11	Lateral Prony vertical	ASC 4421MF-010G	10	27.50
C12	Vertical foundation	ASC 4421-002G	2	102.20
C13	Horizontal foundation	ASC 4421-002G	2	102.20
C14	Case electric motor	ASC 4421-002G	2	102.20

Figure 11 Minimum inertia configuration tested at maximum speed

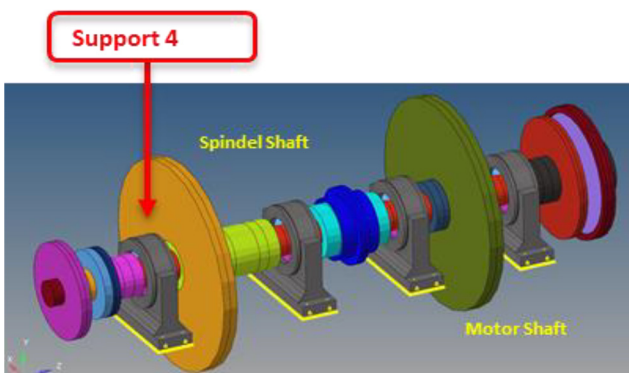


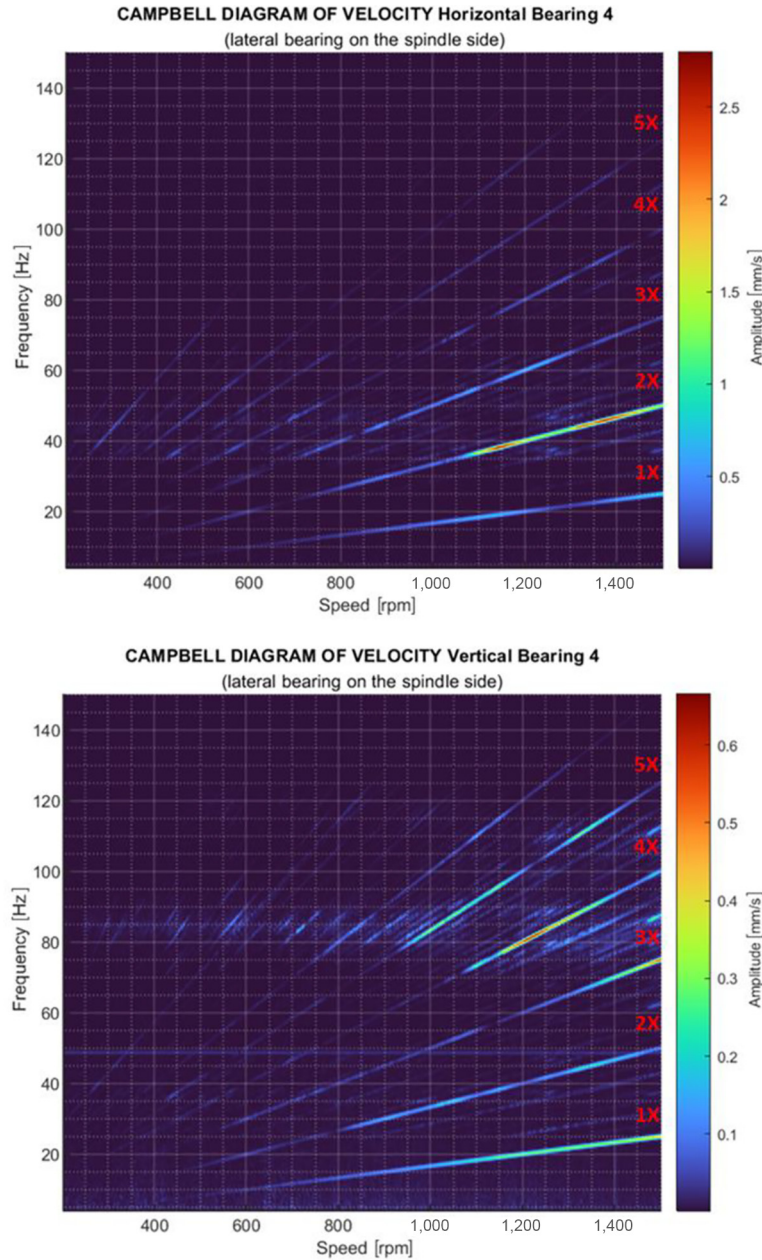
Table 3 Data acquisition parameters for frequency response evaluation

Parameter	Value	Parameter	Value
Sampling frequency	4,000 Hz	Window	2 ¹³ Samples
Filter	Butter 3°	Windowing	Hanning
Overlapping	50%	Algorithm	Fast DFT

have been performed with smooth ramps corresponding to a rig acceleration of 0.8 rpm/s.

In Figure 12, it is represented by the spectrum of velocity rms $v_{4rms}(\omega, \Omega)$ [equation (4)] measured on a support (bearing 4 in Figure 9) with respect to speed Ω of the rig: $v_{4rms}(\omega, \Omega)$ is decomposed in terms of horizontal/transversal (acc.C8) and

Figure 12 Spectrum of velocity rms $v_{4rms}(\omega, \Omega)$ decomposed in terms of $v_{4xrms}(\omega, \Omega)$ (top) and $v_{4yrms}(\omega, \Omega)$ (bottom)



vertical (acc. C7) components, respectively, called $v_{4xrms}(\omega, \Omega)$ [equation (5)] and $v_{4yrms}(\omega, \Omega)$ [equation (6)].

$$v_{4rms}(\omega, \Omega) = \frac{|v_4(\omega, \Omega)|}{\sqrt{2}} \quad (4)$$

$$v_{4xrms}(\omega, \Omega) = \frac{|v_{4x}(\omega, \Omega)|}{\sqrt{2}} \quad (5)$$

$$v_{4yrms}(\omega, \Omega) = \frac{|v_{4y}(\omega, \Omega)|}{\sqrt{2}} \quad (6)$$

On both directions, effects of nonlinear behavior of bearings are evident: harmonic components that are multiple of the synchronous excitation are clearly noticeable.

Dynamic behaviors in vertical and horizontal directions seem to be quite decoupled as maximum values $v_{4x}(\omega)$ and $v_{4y}(\omega)$ are associated to frequencies and speed ranges that are different. This decoupled behavior of vertical and lateral dynamic was also predicted by the preliminary FEM model.

Response of the machine is self-excited by rotor unbalance; exciting forces are proportional to the squared value of rotational speed Ω of the rig. So, it is much more interesting to represent the scaled spectrums of $v_{4x}(\omega)$ and

$v_{4y}(\omega)$, respectively, called $Y_{4x}(\omega)$ [equation (7)] and $Y_{4y}(\omega)$ [equation (8)]:

$$Y_{4x}(\omega, \Omega) = \frac{v_{4xrms}(\omega, \Omega)}{\Omega^2} \quad (7)$$

$$Y_{4y}(\omega, \Omega) = \frac{v_{4yrms}(\omega, \Omega)}{\Omega^2} \quad (8)$$

Behaviors of $Y_{4x}(\omega)$ and $Y_{4y}(\omega)$ are shown, respectively, in Figures 13 and 14: thanks to the proposed scaling with respect to squared speed, it is possible to recognize the presence of two eigen-frequencies on both vertical and lateral planes that are excited by multiple harmonics.

Figure 13 Behavior of $Y_{4x}(\omega, \Omega)$, comparison between modes visible on exp. data and simulation results of simulation FEM model after calibration of bearing stiffness matrix

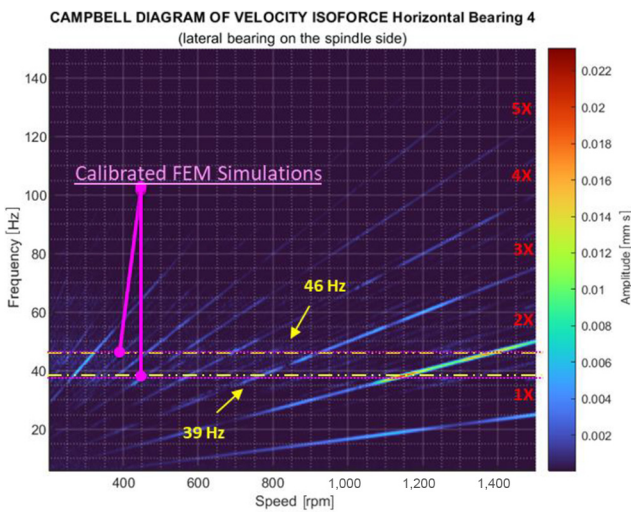
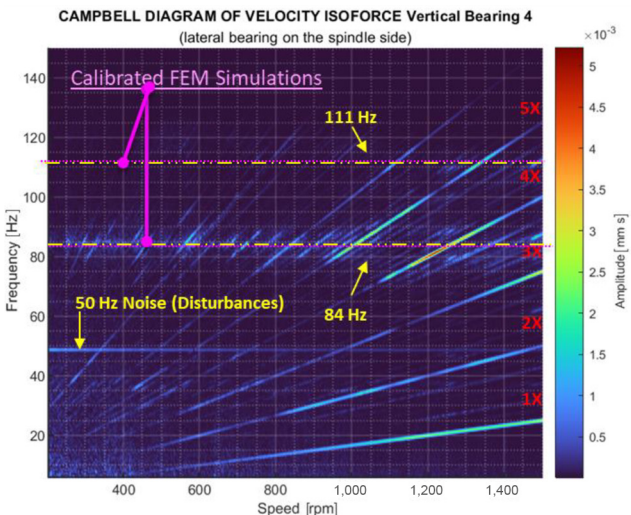


Figure 14 Behavior of $Y_{4y}(\omega, \Omega)$, comparison between modes visible on exp. data and simulation results of simulation FEM model after calibration of bearing stiffness matrix



Measured frequencies on the vertical plane are like the ones foreseen by the finite element model of Figure 8 (further calibration of support model is needed).

The rig is equipped with accelerometers; as visible in Figure 15, the maximum velocity rms recorded during a test is evaluated:

- Highest values of RMS are recorded on Prony beam which is the suspended reaction beam adopted to measure braking torques. These values are not potentially dangerous for the rig: they are referred to as local modes of a flexible structure with limited influence on the rest of the rig.
- Lateral/horizontal vibrations associated to rigid bouncing and tilting modes of the shaft are much more important than vertical ones in terms of recorded vibrations. Bearing 4, which is the nearest to testing area seems to be the more critical one.

4.2 Calibration of bearing stiffness matrix

For a fast calibration of the bearing matrix of the FEM model, authors use the lumped planar model described in Figure 16: the rig shaft is supposed to be rigid, flexible joints between shafts are considered as ideal ones, so every shaft can be studied separately.

Dynamic of the lumped models of Figure 16, is described by equations (9) and (10): tuning its performance by iteratively changing the value of bearing stiffness to fit the values of calculated eigenfrequencies with measured ones. This optimization procedure is performed in Matlab (*fmincon* minimization procedure).

Figure 15 Measured velocity RMS on different measuring points (test at maximum speed, no flywheels installed)

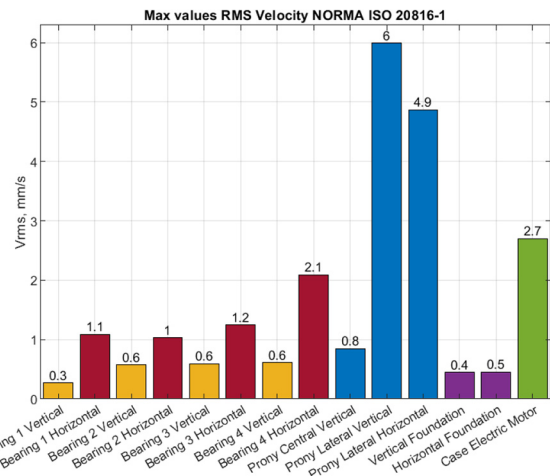
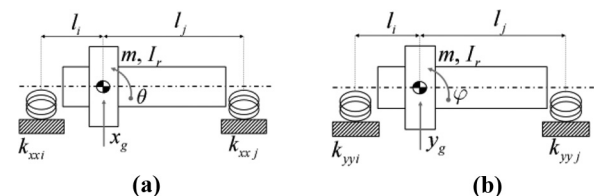


Figure 16 Lumped planar models adopted for the fast identification of the bearing stiffness in (a) transversal directions and (b) vertical one



$$\begin{bmatrix} \dot{x}_g \\ \dot{\theta} \\ \ddot{x}_g \\ \ddot{\theta} \end{bmatrix} = \underbrace{\begin{bmatrix} 0 & 0 & 1 & 0 \\ 0 & 0 & 0 & 1 \\ -\frac{(k_{xxi} + k_{xxj})}{m} & -\frac{(k_{xxj}l_j - k_{xxi}l_i)}{m} & 0 & 0 \\ -\frac{(k_{xxj}l_j - k_{xxi}l_i)}{I_r} & -\frac{(k_{xxj}l_j^2 + k_{xxi}l_i^2)}{I_r} & 0 & 0 \end{bmatrix}}_{A_x} \begin{bmatrix} x_g \\ \theta \\ \dot{x}_g \\ \dot{\theta} \end{bmatrix} \quad (9)$$

$$\begin{bmatrix} \dot{y}_g \\ \dot{\varphi} \\ \ddot{y}_g \\ \ddot{\varphi} \end{bmatrix} = \underbrace{\begin{bmatrix} 0 & 0 & 1 & 0 \\ 0 & 0 & 0 & 1 \\ -\frac{(k_{xxi} + k_{xxj})}{m} & -\frac{(k_{xxj}l_j - k_{xxi}l_i)}{m} & 0 & 0 \\ -\frac{(k_{xxj}l_j - k_{xxi}l_i)}{I_r} & -\frac{(k_{xxj}l_j^2 + k_{xxi}l_i^2)}{I_r} & 0 & 0 \end{bmatrix}}_{A_y} \begin{bmatrix} y_g \\ \varphi \\ \dot{y}_g \\ \dot{\varphi} \end{bmatrix} \quad (10)$$

Lateral and vertical stiffness of four supports are identified.

All supports are equal (same bearing model). The linear law visible in Figure 17 fits the measured behavior of bearing stiffness with respect to applied loads.

Each support is loaded in a different way: maximum stiffness of the most loaded support is four to five times higher than the minimum one. So performed identification of the real stiffness of the supports with respect to their real loading and assembly conditions is fundamental. This new calibrated model of support stiffness is applied to the FEM model of the rig. In following sections of this work, results of the FEM calibrated model are compared with the real behavior of the rig.

4.3 Identification of equivalent damping ratio

Most of the damping of the rig is provided by bearings. Calculation and identification of damping of lubricated roller bearings is still object of active research (Wu et Al., 2008; Tsucha and Cavalca, 2020).

For this reason, authors preferred to evaluate the equivalent damping of the system from the measured response of ramp tests.

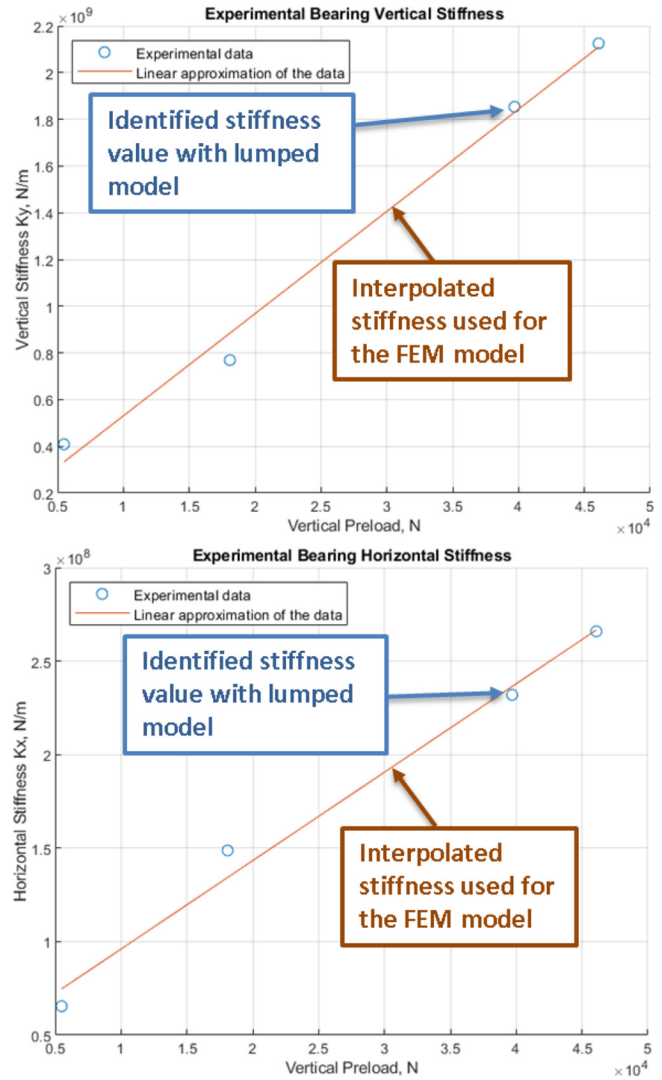
Half power method is applied to the measured response of a mode as visible in Figure 17: the mode is self-excited by the unbalance of the machine, and it is slightly damped. So, it can be assumed that exciting forces are almost constant over the considered variation of rotation speed of the rig.

Applying the half power method (Ewins, 2009) the damping coefficient of the mode can be calculated according to equation (11): f_r , f_1 and f_2 are, respectively, the resonant frequency and corresponding half power frequencies in which amplitude is reduced to a $\sqrt{2}$ factor.

$$\xi = \frac{f_2 - f_1}{2f_r} \quad (11)$$

Once the damping factor of the modes is calculated, it is possible to adjust the damping coefficients of supports to obtain the desired damping of simulated modes.

Figure 17 Calibrated stiffness behavior obtained interpolating results of the identification performed with the lumped model of Figure 15



4.4 Impulse response test

Ramp tests cannot properly excite all the modes of the rig, especially for rig configurations in which all the flywheels are installed. When flywheels are installed rotating speed of the rig is limited and the center of mass of the shaft is substantially centered with respect to supports, so excitation of rigid tilting modes is also limited. This mode foreseen by the finite element model is almost unrecognizable on ramp tests.

For these reasons, the rig in standstill conditions is excited with an impulsive force using a hammer as visible in Figure 19.

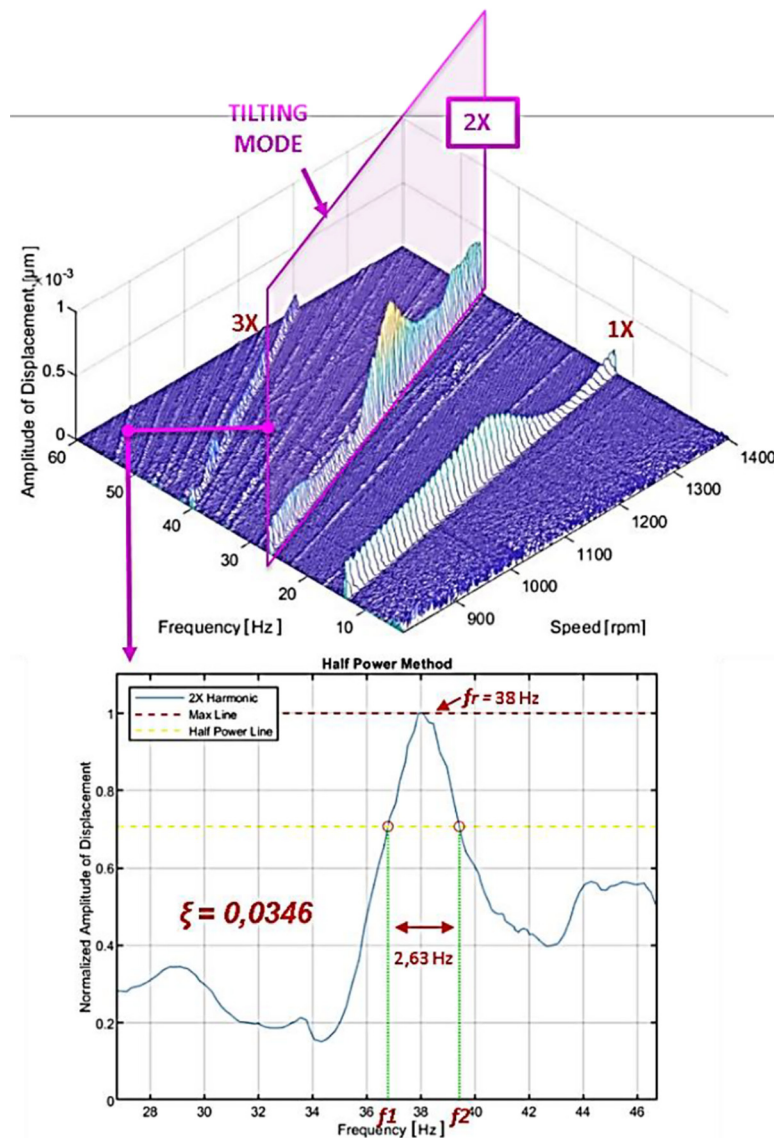
Test is repeated for two different loading configurations:

- 1 The “naked” configuration in which no flywheels are installed.
- 2 Full inertia – all the flywheels are installed.

In Figure 18, some results referred on accelerations measured on support 4 for both rig configurations are shown:

- For the “naked” configuration the same tilting and bouncing mode recorded on ramp tests and foreseen by FEM model

Figure 18 Identification of equivalent damping adopting the half power method to the analysis of a tilting mode (measurements are referred to support 4)



are recognizable. Calculated FEM modes considered in Figure 20 are calculated considering the calibrated stiffness of bearings visible in Figure 17.

For the configuration with maximum inertia (all flywheels installed), proposed impulsive input excites a horizontal tilting mode at 41 Hz. This is the same frequency foreseen by the finite element model of the rig (after the calibration of bearings).

In Table 4, authors have summarized the comparison of identified eigen frequencies of the spindle shaft with corresponding modes calculated by the finite element model calibrated with stiffness and damping of bearings, respectively, defined in Figures 17 and 18. Validation is performed on a limited number of rigid modes that authors were able to excite with ramp tests (naked rotor) or with hammer tests.

Calibrated FEM model fit well experimental data. Calibration of bearing stiffness was performed with the planar

rigid model of Figure 16: this is a further confirmation that the dynamic of the rig is mainly described by low frequency rigid modes which are almost planar.

Tests are repeated with different configurations of installed inertia. As shown in Table 4, errors between identified modes and simulated ones are higher for the configuration with installed flywheel. This result can be easily explained considering the following aspects:

- Hammer impulse is always the same, but the inertia of the rig is much higher when flywheel 4 is installed. So, the input is relatively much smaller with respect to the system that must be identified, higher errors in identified modes are a feasible consequence.
- When flywheel is installed, weight on supports and conversely frictions are higher. Higher frictions involve higher distortions on identified modes if input excitation is relatively small.

Figure 19 Application of lateral impulsive forces to excite tilting modes of the rig

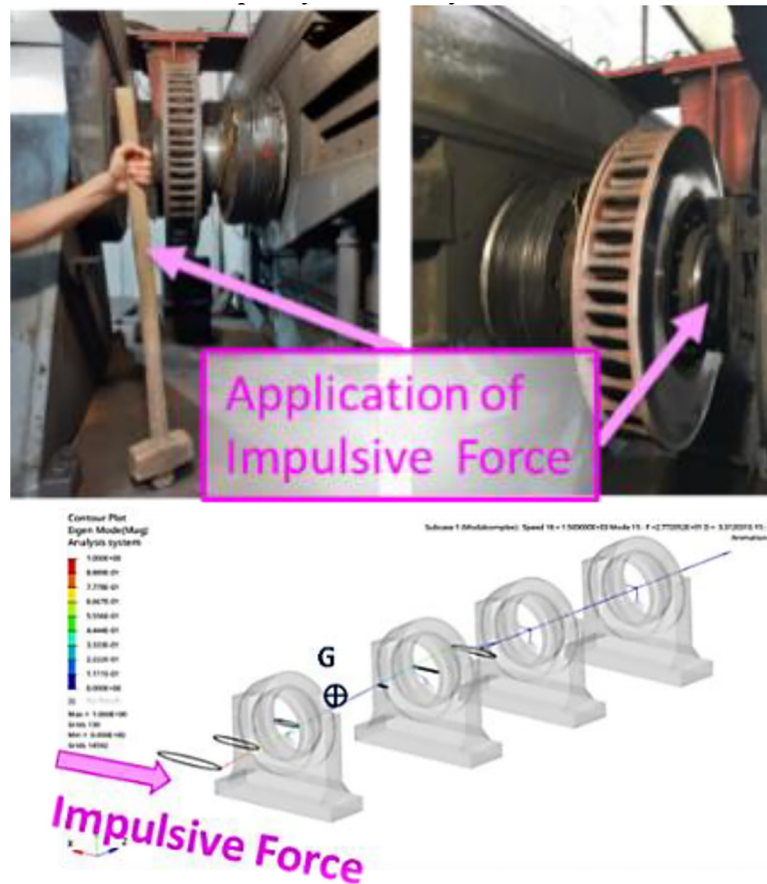
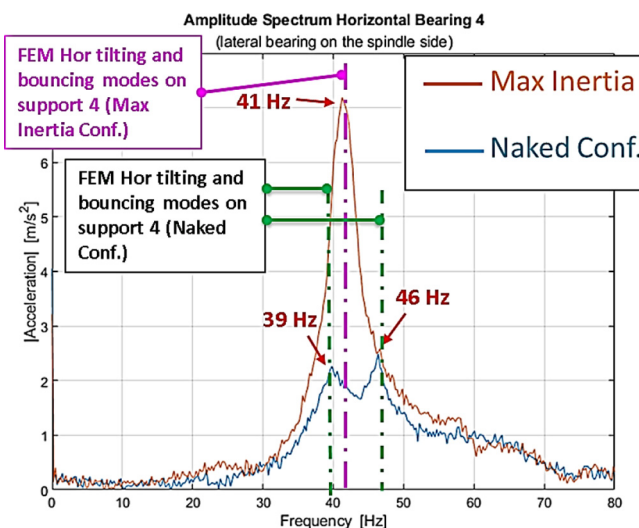


Figure 20 Identification of equivalent damping adopting the half power method to the analysis of a tilting mode (measurements are referred to support 4)



- The flywheel is attached to the rotor with a flange. FEM model reproduces this constraint; however, some light approximations in modeling are probably introduced (preloads and friction between rotor flange and flywheel).

To make clear the description, some modal shapes (naked rotor configuration) listed in Table 4 are represented in Figure 21.

4.5 Braking tests

Realistic brake tests are performed to verify the applicability of proposed methodologies while the rig is working.

In Figure 22, it is shown an example of obtained results in terms of measured vibrations of bearing 4 (the most critical in term of vibrations): during the braking tests decelerations are much higher with respect to free ramp tests (a braking test has a duration of 1–2 min). Application and the modulation of braking forces during the tests introduce some further flexo-torsional disturbances. However, as visible in Figure 22, behavior of recorded vibrations is still quite like the one recorded in free ramp tests shown in Figure 12. Maximum vibrations on bearing 4 (the spindle one which is the more critical) are recorded when the rig is traveling at 1,384 rpm: in this condition, the second harmonic excites a mode that according to the finite element model is the transversal bouncing one.

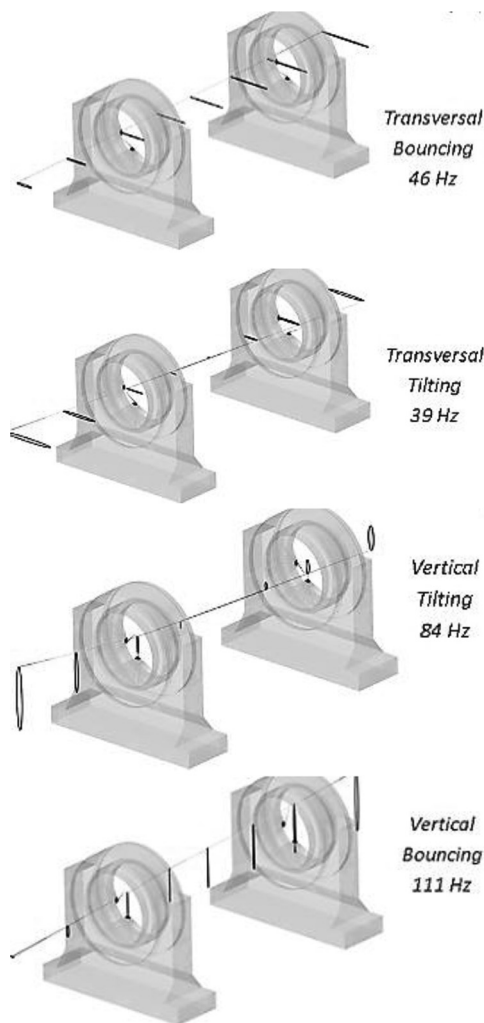
From experimental measurements authors were able to reconstruct approximated displacements of supports using the following procedure:

- Spectrum of measured accelerations on supports is calculated; static and high frequency noise components are filtered.

Table 4 Data acquisition parameters for frequency response evaluation (modes of spindle shaft)

Rig configuration	Modal shape (description)	Exp. frequency	FEM frequency (calibrated Model)	Absolute error	Relative error (%)
Naked rotor (No flywheel on the rotor)	Rigid tilting on transversal plane	39 Hz	38.6 Hz	0.4 Hz	1
	Rigid bouncing on transversal Plane	46 Hz	47.4 Hz	-1.4 Hz	-3
	Rigid tilting on vertical plane	84 Hz	84.2 Hz	-0.2 Hz	-0.2
	Rigid bouncing on vertical plane	111 Hz	111.9 Hz	-0.9 Hz	-0.8
Rotor with flywheel 4 (1, 625kg/m ²)	Rigid tilting on transversal plane	41 Hz	38.3 Hz	2.7 Hz	6.6
	Rigid bouncing on transversal plane	35 Hz	36.6 Hz	-1.6 Hz	-4.6
	Rigid tilting on vertical plane	75 Hz	77.1 Hz	-2.1 Hz	-2.8
	Rigid bouncing on vertical plane	95 Hz	94.6 Hz	0.4 Hz	0.4

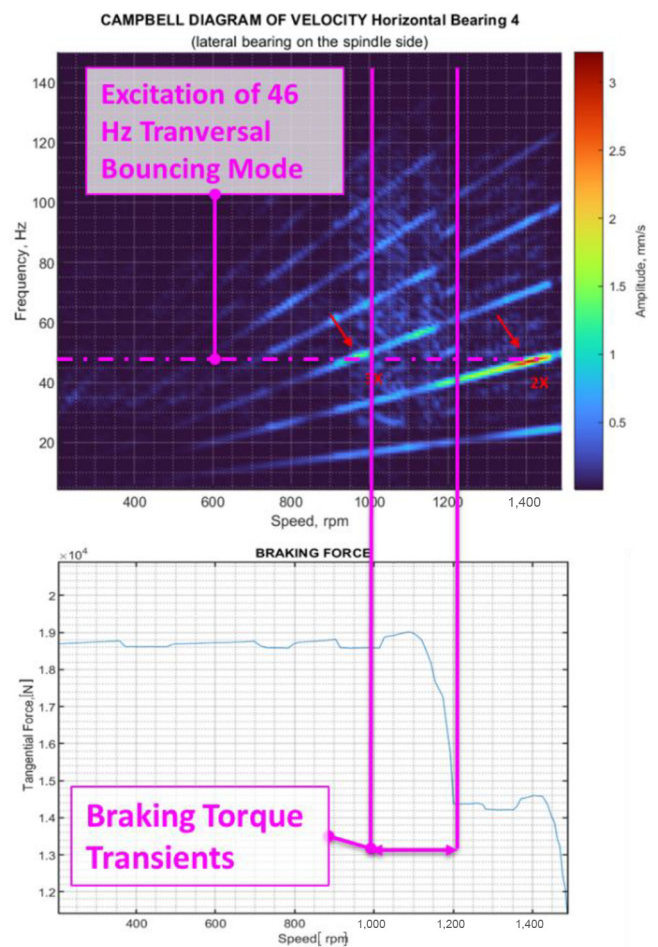
Figure 21 Calculated modal shapes of the spindle shaft (calibrated finite element model) for the naked rotor configuration



- Each frequency component is integrated two times (considering the phase of each frequency contribution).
- Corresponding spectrum of displacements is converted back in time domain signals.

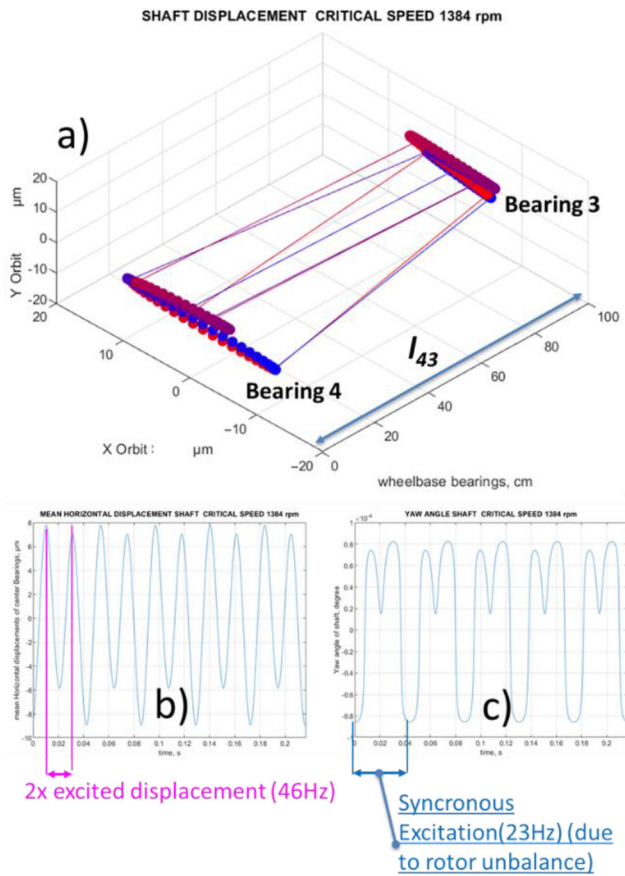
By integrating measurement of both vertical and lateral accelerometers 3 and 4, it was possible to reconstruct equivalent

Figure 22 Example of results during a real braking test



transversal (x_3, x_4) and vertical (y_3, y_4) displacements of supports. In Figure 23(a), these displacements are shown: results are referred to the instant in which the rig is rotating at 1,384 rpm (23 Hz) and max vibrations at 46 Hz are recorded. Displacements of supports are coherent with the excitation of the transversal bouncing mode at 46 Hz that is described by the FEM model in Figure 21. Using this approach, authors were able to reconstruct the mean displacement of the supports x_m defined [equation (12)] as the arithmetic mean of transversal

Figure 23 Reconstructed behavior of displacements on (a) supports (b) including x_m and (c) ψ_m



displacements of the supports 3 and 4, respectively, called x_3 and x_4 . An equivalent yaw angle ψ_m is defined [equation (13)] as the ratio between the difference between x_3 and x_4 and the axial distance between the two supports l_{43} .

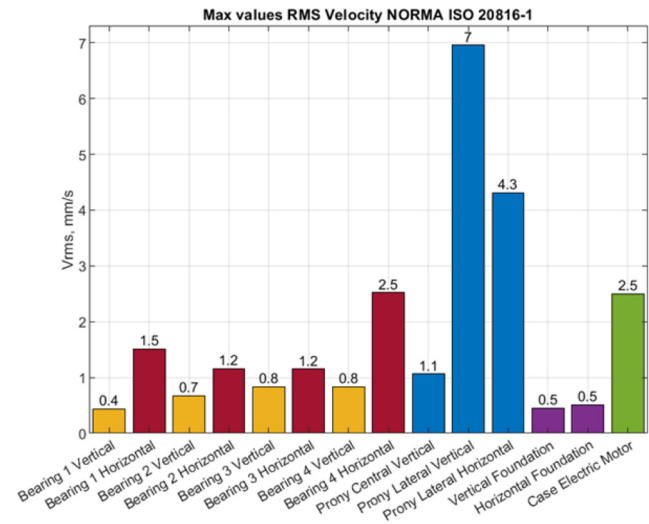
$$x_m = \frac{x_4 + x_3}{2} \tag{12}$$

$$\psi_m = \frac{x_4 - x_3}{l_{43}} \tag{13}$$

Behaviors of both x_m ψ_m are shown in Figure 23(b) and (c): reconstructed x_m corresponds to a near to sinusoidal motion at 46 Hz while the difference angle ψ_m is substantially a synchronous oscillation at 23 Hz probably excited by rotor unbalance. All these evaluations confirm that supports are vibrating on a transversal plane with a shape that is substantially coherent with the modal behavior predicted by the FEM model.

Maximum value of recorded rms of vibration speed during a braking test are shown in Figure 24: results are quite like the one obtained on free ramp tests (see Figure 15). The level of recorded vibration is a bit higher, but the trend is almost the same: highest levels of vibrations are measured on the Prony beam that support brake clamps. However, potential risk and danger of vibrations on Prony beam is limited. On supports, higher level of vibrations is measured on bearing 4 and are mainly associated to rigid modes in transversal/horizontal direction.

Figure 24 Measured velocity RMS on different measuring points (braking test at maximum speed, no flywheels installed)



5. Possible improvements of monitoring system of rig supports

Models and tests performed on the Italcertifer test rig indicate that higher level of vibrations is mainly related to rigid modes. This modal behavior is mainly influenced by compliant supports.

Observed rigid modes are associated to tilting and bouncing movements that are performed with respect to vertical and transversal planes. Modes on vertical and transversal planes are substantially decoupled. Supports are preloaded in vertical direction, so frequencies that are mostly excited are in transversal/horizontal direction.

For diagnostic purposes wear of bearings, typically produces increased clearances and consequently an amplification of these low frequency rigid modes.

Diagnostic systems installed not only on Italcertifer test rigs but more generally on this kind of machines are typically based on vertical accelerometers or velocimeters placed on supports. Consequently, installed diagnostic systems are less sensitive in the direction which is typically associated to higher vibration levels.

This configuration of diagnostic systems is largely suboptimal, and it can be improved in two ways:

- 1 It is possible to maintain a simpler diagnostic system in which each support is monitored by a single accelerometer or velocimeter. In this case, the orientation of this single channel sensor must be optimized to be sensitive to vibrations in different directions or alternatively in the horizontal one. Also, more cautious diagnostic thresholds can be adopted.
- 2 Alternatively, it is possible to install on supports, multichannel sensors are able to completely reconstruct module and direction of vibrations as the experimental system that has been adopted in this work to identify the rig.

6. Conclusions and future developments

In this work, vibrational behavior of a dynamometric test rig for railway brakes has been investigated. The activity is performed

on an industrial relevant case study, one of the test rigs that is officially homologated by UIC for brake testing.

Aim of the activity was the development of a tailored identification procedure that can be applied with a null or negligible impact on the productivity of the rig that must perform thousands of simulated braking tests every year.

Finite element modeling suggested that vibrations recorded on rig supports are due to the excitation of rigid modes due to the anisotropic compliance of bearings.

Uncertain parameters such as equivalent stiffness and damping of the bearings have been identified experimentally with a combination of tests (slow ramp test and impulse excitation test) that allows to identify separately both parameters without affecting the normal use of the rig. Further measurements performed on real braking test have confirmed the validity of the suggested approach giving useful indications regarding the monitoring of the vibrations measured on rig supports transversal bouncing and tilting oscillations are the lowest and most frequently excited modes, so the disposition of accelerometers installed on rig supports should be modified accordingly as current monitoring systems installed on these rigs are substantially designed to measure vertical vibrations. This is a simple but clear innovation with respect to current state of the art. Also proposed procedure is clearly extendable to the other homologated test rig whose design criteria are converging as they are designed to perform the same standardized testing procedures.

Currently, authors are prosecuting their activities also on other plants like the new test dynamometric test rig of Firenze Osmannoro, where maximum speed is higher (3,000 rpm corresponding to 500 km/h). Also, smaller rigs adopted for the automotive sector should be the object of future activities. Aim of these activities is to further generalize the approach proposed in this work to a wider population of machines. Authors are also evaluating the possibility of introducing a more accurate computational fluid dynamics study of thermal exchanges and ventilation effect on both tested brakes and rigs. For these future developments, an interesting contribution is represented by recent works of [Shoeibi et al. \(2022a, 2022b\)](#) and [Hoseinzadeh and Heyns \(2020\)](#).

References

- Alemanı, M., Wahlström, J., Matějka, V., Metinöz, I., Söderberg, A., Perricone, G. and Olofsson, U. (2018), "Scaling effects of measuring disc brake airborne particulate matter emissions—A comparison of a pin-on-disc tribometer and an inertia dynamometer bench under dragging conditions", *Journal of Engineering Tribology*, Vol. 232 No. 12, pp. 1538-1547.
- Bian, G. and Wu, H. (2016), "Friction surface structure of a cf/C-SiC composite brake disc after bedding testing on a full-scale dynamometer", *Tribology International*, Vol. 99, pp. 85-95.
- Borawski, A. (2019), "Common methods in analysing the tribological properties of brake pads and discs: a review", *Acta Mechanica Et Automatica*, Vol. 13 No. 3.
- Bracciali, A. and Megna, G. (2018), "Solving groan noise problems in a metro braking system", *Proceedings of The Fourth International Conference on Railway Technology, Railways 2018, Sitges, Barcelona*, pp. 3-7.
- Dadouche, A., Rezaei, A., Wickramasinghe, V., Dmochowski, W., Bird, J.W. and Nitzsche, F. (2008), "Sensitivity of air-coupled ultrasound and eddy current sensors to bearing fault detection", *Tribology Transactions*, Vol. 51 No. 3, pp. 310-323.
- Donelson, J., III. and Dicus, R.L. (2002), "Bearing defect detection using on-board accelerometer measurements", *ASME/IEEE Joint Rail Conference 2002 Jan 1*, Vol. 35936, pp. 95-102.
- Duan, Z., Wu, T., Guo, S., Shao, T., Malekian, R. and Li, Z. (2018), "Development and trend of condition monitoring and fault diagnosis of multi-sensors information fusion for rolling bearings: a review", *The International Journal of Advanced Manufacturing Technology*, Vol. 96 Nos 1/4, pp. 803-19.
- Ehret, M. (2021), "Identification of a dynamic friction model for railway disc brakes", *Part F: Journal of Rail and Rapid Transit*, Vol. 235 No. 10, pp. 1214-1224.
- Ewins, D.J. (2009), *Modal testing: theory, Practice and Application*, John Wiley & Sons, New York, NY.
- Fag Pro Check Monitoring System (2022), available at: www.ien.eu/article/fag-procheck-monitoring-system/
- Fan, Z.Y. (2021), "Systems", *Tribology Letters*, Vol. 69 No. 1, pp. 1-19.
- Gehrig, R., Hill, M., Lienemann, P., Zwicky, C.N., Bukowiecki, N., Weingartner, E. and Buchmann, B. (2007), "Contribution of railway traffic to local PM10 concentrations in Switzerland", *Atmospheric Environment*, Vol. 41 No. 5, pp. 923-933.
- Hemmati, F., Orfali, W. and Gadala, M.S. (2016), "Roller bearing acoustic signature extraction by wavelet packet transform, applications in fault detection and size estimation", *Applied Acoustics*, Vol. 104, pp. 101-118.
- Hoseinzadeh, S. and Heyns, P.S. (2020), "Thermo-structural fatigue and lifetime analysis of a heat exchanger as a feedwater heater in power plant", *Engineering Failure Analysis*, Vol. 113, p. 104548.
- IRS0548 (2020), "Requirements of friction test benches for the international certification of brake pads and brake blocks", Author UIC 1st release 2020.
- ISO 20816-1 (2016), "Mechanical vibration – measurement and evaluation of machine vibration – part 1: general guidelines", available at: www.iso.org/standard/63180.html
- Kim, K.I., Lee, H., Kim, J., Oh, K.H. and Kim, K.T. (2021), "Wear Behavior of commercial copper-based aircraft brake pads fabricated under different SPS conditions", *Crystals*, Vol. 11 No. 11, p. 1298.
- Kurvinen, E., Viitala, R., Choudhury, T., Heikkinen, J. and Sopanen, J. (2020), "Simulation of subcritical vibrations of a large flexible rotor with varying spherical roller bearing clearance and roundness profiles", *Machines*, Vol. 8 No. 2, p. 28, doi: [10.3390/machines8020028](https://doi.org/10.3390/machines8020028).
- Lyu, Y., Bergseth, E., Tu, M. and Olofsson, U. (2018), "Effect of humidity on the tribological behaviour and airborne particle emissions of railway brake block materials", *Tribology International*, Vol. 118, pp. 360-367.
- Malla, C. and Panigrahi, I. (2019), "Review of condition monitoring of rolling element bearing using vibration

- analysis and other techniques”, *Journal of Vibration Engineering & Technologies*, Vol. 7 No. 4, pp. 407-414.
- Mann, R., Magnier, V., Brunel, J.F., Dufrenoy, P., Henrion, M. and Guillet-Revot, E. (2021), “Thermomechanical characterization of high-speed train braking materials to improve models: numerical validation via a comparison with an experimental braking test”, *Tribology International*, Vol. 156, p. 106818.
- Nirwan, N.W. and Ramani, H.B. (2022), “Condition monitoring and fault detection in roller bearing used in rolling mill by acoustic emission and vibration analysis”, *Materials Today: Proceedings*, Vol. 51, pp. 344-54.
- Presciani, P., Rinchi, M. and Pugi, L. (2003), “Banchi per la certificazione dei componenti frenanti (2003)”, *Ingegneria Ferroviaria*, Vol. 58 No. 3, pp. 285-294.
- Pugi, L. and Abati, A. (2020), “Design optimization of a planar piezo-electric actuation stage for vibration control of rotating machinery (2020)”, *Meccanica*, Vol. 55 No. 3, pp. 581-596, doi: [10.1007/s11012-020-01129-x](https://doi.org/10.1007/s11012-020-01129-x).
- Pugi, L., Malvezzi, M., Papini, S. and Tesi, S. (2015), “Simulation of braking performance: the AnsaldoBreda EMU V250 application (2015)”, *Journal of Rail and Rapid Transit*, Vol. 229 No. 2, pp. 160-172, doi: [10.1177/0954409713504394](https://doi.org/10.1177/0954409713504394).
- Randall, R.B. (2021), *Vibration-Based Condition Monitoring: industrial, Automotive and Aerospace Applications*, John Wiley & Sons, New York, NY.
- Sawczuk, W., Cañas, A.M., Ulbrich, D. and Kowalczyk, J. (2021), “Modeling the average and instantaneous friction coefficient of a disc brake on the basis of bench tests”, *Materials*, Vol. 14 No. 16, p. 4766.
- Sawczuk, W. and Jüngst, M. (2019), “Numerical analysis and testing of a new segmented brake disc fixed to the wheel of a wheelset”, *Problemy Kolejnictwa*, Vol. 183, pp. 121-135.
- Shoeibi, S., Ali Agha Mirjalily, S., Kargarsharifabad, H., Panchal, H. and Dhivagar, R. (2022a), “Comparative study of double-slope solar still, hemispherical solar still, and tubular solar still using Al₂O₃/water film cooling: a numerical study and CO₂ mitigation analysis”, *Environmental Science and Pollution Research*, Vol. 29, pp. 1-17.
- Shoeibi, S., Rahbar, N., Abedini Esfahlani, A. and Kargarsharifabad, H. (2022b), “Energy matrices, economic and environmental analysis of thermoelectric solar desalination using cooling fan”, *Journal of Thermal Analysis and Calorimetry*, Vol. 147 No. 17, pp. 1-16.

- Shuai, Z., Gao, F. and Fu, R. (2019), “Study of electric simulation inertia range for train braking test dynamometer”, *Journal of Dalian Jiaotong University*, Vol. 3.
- Simpro Quick Pro (2022), “User guide and tech references”, available at: www.skf.com/it/support/engineering-tools/simpro-quick
- Tomovic, R., Miltenovic, V., Banic, M. and Miltenovic, A. (2010), “Vibration response of rigid rotor in unloaded rolling element bearing”, *International Journal of Mechanical Sciences*, Vol. 52 No. 9, pp. 1176-1185.
- Tsuha, N.A.H. and Cavalca, K.L. (2020), “Stiffness and damping of elastohydrodynamic line contact applied to cylindrical roller bearing dynamic model”, *Journal of Sound and Vibration*, Vol. 481, p. 115444.
- UIC 541-3:Brakes (2017), “Disc brakes and their applications –general conditions for the certification of brake parts”.
- UIC 548 Brakes (2020), “Requirements of friction test benches for the international certification of brake pads and brake blocks”, *Annex I: UIC approved friction test benches*, last update 18/09/2020, available at: https://uic.org/IMG/pdf/uic_leaflet_548_appendix_i_09-2020.pdf
- Wang, W.J., Wang, F., Gu, K.K., Ding, H.H., Wang, H.Y., Guo, J. and Zhu, M.H. (2015), “Investigation on braking tribological properties of metro brake shoe materials”, *Wear*, Vols 330/331, pp. 498-506.
- Wang, Z., Han, J., Domblesky, J.P., Li, Z., Fan, X. and Liu, X. (2019), “Crack propagation and microstructural transformation on the friction surface of a high-speed railway brake disc”, *Wear*, Vols 428/429, pp. 45-54.
- Wu, H., Wang, J.-W. and Qi, A.N. (2008), “Calculating method for damping of cylindrical roller bearings”, *Bearing*, Vol. 9, pp. 1-5.
- Yanar, H., Purcek, G., Demirtas, M. and Ayar, H.H. (2022), “Effect of hexagonal boron nitride (h-BN) addition on friction behavior of low-steel composite brake pad material for railway applications”, *Tribology International*, Vol. 165, p. 107274.
- Yevtushenko, A., Kuciej, M. and Wasilewski, P. (2019), “Experimental study on the temperature evolution in the railway brake disc”, *Theoretical and Applied Mechanics Letters*, Vol. 9 No. 5, pp. 308-311.

Corresponding author

Luca Pugi can be contacted at: luca.pugi@unifi.it